Nuclear Instruments and Methods in Physics Research A 592 (2008) 420–427

Contents lists available at ScienceDirect

Nuclear Instruments and Methods in Physics Research A

journal homepage: www.elsevier.com/locate/nima

Polarimetric neutron spin echo: Feasibility and first results

C. Pappas [a,*], E. Lelièvre-Berna [b], P. Bentley [a,1], E. Bourgeat-Lami [b], E. Moskvin [a,c], M. Thomas [b], S. Grigoriev [c], V. Dyadkin [c]

[a] Hahn-Meitner Institut Berlin, Glienickerstr. 100, 14109 Berlin, Germany
[b] Institut Laue-Langevin, 6, Rue Jules Horowitz, 38042 Grenoble, France
[c] PNPI, 188300 Gatchina, Leningrad District, Russia

ARTICLE INFO

Article history:
Received 24 October 2007
Received in revised form
22 April 2008
Accepted 27 April 2008
Available online 10 May 2008

Keywords:
Neutron scattering
Spin arrangements determination
Neutron spectroscopy

ABSTRACT

Neutron Spin Echo (NSE) spectroscopy uses polarized neutrons and accordingly polarization analysis is an intrinsic feature of NSE. However, the multifaceted dynamics of antiferromagnets and helimagnets require more than the classical NSE set-up. Here we present the feasibility test and first results of a new and powerful technique: Polarimetric NSE, obtained by combining the wide angle NSE spectrometer SPAN, developed at HMI with the zero-field polarimeter Cryopad developed at ILL.

1. Introduction

The scattering of neutrons from the electronic spins arises from the magnetic dipole–dipole interaction and is fundamentally different from the nuclear spin-flip scattering, which is mediated by the strong nuclear interaction. As Blume and Maleyev showed in 1963 almost simultaneously, neutrons see only those electronic spin components that are perpendicular to the scattering vector $\vec{Q}$ [1,2]. The magnetic scattering cross-section can be decomposed into a "normal" magnetic, a chiral magnetic and a nuclear-magnetic interference component. The "normal" magnetic component leads to a 180° rotation of the neutron beam polarization around the magnetic interaction vector, and therefore a spin-flip scattering, when the incident neutron beam polarization $\vec{P}_i$ is parallel to $\vec{Q}$. The effect of the chiral magnetic and nuclear-magnetic interference components is more subtle as they may lead to a rotation of the polarization vector, and the intensity may vary with the direction of the incident polarization. We invite the reader to watch the movies available at ⟨http://www.ill.eu/sane/⟩ for a better understanding of the polarization behavior.

The theoretical results of Blume and Maleyev were very soon followed by the historical experiment of Moon, Riste and Köhler in 1969 [3], who used a polarizer, a spin flipper and an analyzer to measure the spin-flip and non-spin-flip channels, respectively. Large adiabatic magnetic fields guided the polarization through the spectrometer so that only the projection of the polarization along these fields could be analyzed. This was the first longitudinal polarization analysis (LPA) set-up and the genesis of a successful technique with a broad range of applications. LPA can be one directional as in Ref. [3] or three directional, with the incident polarization rotated towards the three perpendicular directions *x*, *y* and *z*, as first suggested by Mezei [4]. However, the limitations of this powerful technique become obvious when dealing with chiral magnetic systems or with systems with nuclear-magnetic interferences, where LPA cannot distinguish between a simple depolarization resulting from, e.g. magnetic domains and a rotation of the polarization vector resulting from chiral or nuclear-magnetic interference terms.

For several years polarization analysis and LPA were synonyms. Nevertheless, already in the early 1970s first arrangements were developed with a zero-field area around the sample and accessing components of the final polarization transverse to the incoming polarization [5–7]. The zero-field chamber approach was born, but found limited use, mostly around the direct beam. The situation changed with the development of the Cryopad at ILL [8], which is based on Meissner shields and provides access to any angle of the scattering vector $\vec{Q}$, e.g. on a three-axis spectrometer or a diffractometer. The notion of Spherical Neutron Polarimetry (SNP) emerged with Cryopad being able to do the most generalized polarization analysis experiments and to measure any theoretically possible pair-correlation function at any point of the reciprocal space. The recent developments have led to a third generation

* Corresponding author.
E-mail address: pappas@hmi.de (C. Pappas).
[1] Present address: Institut Laue-Langevin, 6, Rue Jules Horowitz, 38042 Grenoble, France.

0168-9002/$ - see front matter © 2008 Elsevier B.V. All rights reserved.
doi:10.1016/j.nima.2008.04.078

Cryopad, a highly flexible and reliable system with the Meissner shields protected by additional μ-metal screens [9]. Recently similar systems have also been realized on the basis of μ-metal screens without any Meissner shields [10], but do not achieve the resolution, reliability and stray-field insensitivity of Cryopad.

Neutron Spin Echo (NSE) spectroscopy emerged in the early 1970s and was a revolutionary technique at that time as it is exclusively based on the transverse components of the polarization [11]. NSE uses the Larmor precession of neutron spins in a magnetic field to directly measure the energy transfer at the sample and it decouples the energy resolution from beam characteristics like monochromatization and collimation. Larmor labeling requires polarized neutrons and accordingly polarization analysis is an integral part of NSE [4]. The "normal" magnetic cross-section acts as a π-flipper and creates an echo without the otherwise obligatory π-flipper at the sample. This leads to a straightforward and unambiguous separation of the magnetic and the nuclear signal and have made it possible to perform NSE also on disordered and diluted magnetic systems, like random antiferromagnets and spin glasses, where the magnetic scattering often is a small fraction of the total signal due to structural contributions

In NSE the precession magnetic field is applied over the entire spectrometer. Given the broad monochromatization, the Larmor precessions depolarize the beam at the sample, where the neutron spins are uniformly distributed over the precession plane perpendicular to the field. The situation is straightforward for the "normal" magnetic cross-section [4], but gets extremely complicated in the presence of chiral and nuclear-magnetic interference terms. In such complex cases it is difficult to completely understand and analyze the experimental results. The way out is the Polarimetric NSE set-up, which combines the precession field areas required for NSE spectroscopy with the zero-field sample chamber and the precession units of the Cryopad. Here we present a first realization of such a set-up using the third generation Cryopad and a modified version of the Intensity Modulated Variant of NSE (IMNSE) [12].

2. Method and instrumental approach

The equation of motion of the magnetic moments of neutrons $\vec{\mu}$ in a magnetic field $\vec{H}$ is

$$\frac{\mathrm{d}\vec{\mu}}{\mathrm{dt}} = -\gamma\vec{\mu}\times\vec{H} = \vec{\mu}\times\vec{\omega}_L \tag{1}$$

where $\gamma = \gamma_n/2\pi = 29.16\,\mathrm{MHz/T}$, γ_n is the gyromagnetic ratio of the neutron and $\omega_L = \gamma H$ the Larmor precession frequency. Eq. (1) is the starting point of a widely used classic description of NSE spectroscopy [11]. Neutrons have a spin 1/2 and Larmor precession results from the coherent interference between the $|+\rangle$ and the $|-\rangle$ states in a magnetic field. A quantum mechanical description of NSE can be found in Refs. [13,14].

An extensive description of the different NSE configurations is given in Ref. [15]. The classic sequence of an NSE measurement is as follows:

Polarizer − $\pi/2$ flipper − Precession Field − $-\pi$ flipper (Sample)− Precession Field − $\pi/2$ flipper − Analyzer

The $\pi/2$-flippers are fundamental in NSE spectroscopy: they rotate the beam polarization by $\pi/2$ and mark the beginning and the end of the precession field areas. With a magnetic field of a strength H and a length ℓ the precession angle ϕ of each spin is proportional to t, the time the neutron spends in the field:

$$\phi = \gamma H t = \frac{\gamma H \ell}{v} = \frac{\gamma m}{h} H \ell \lambda = aI\lambda \tag{2}$$

where m is the mass of the neutron, $a = \gamma m/h$ and I the magnetic field integral. The precession angle records the velocity of the individual neutron and is proportional to the neutron wavelength. The Larmor precessions lead to a wavelength-dependent beam polarization:

$$P = P_0\cos(aI\lambda) \tag{3}$$

A distribution of neutron wavelengths induces a distribution of precession angles and a typical monochromatization of 10–20%, as commonly used in NSE spectroscopy, completely depolarizes the beam shortly behind the $\pi/2$-flipper. The π-flipper at the sample is the symmetry point of the spectrometer. It marks the reversal point of the precessions so that the NSE signal can be recovered at the last $\pi/2$-flipper. As pointed out previously, in the case of paramagnetic NSE the π-flipper is not needed, because the sample itself acts as a π-flipper.

The decoupling of the precessions from the sample area is achieved by two additional $\pi/2$-flippers: one in front and one behind the sample, and results in the so-called ferromagnetic NSE sequence:

Polarizer − $\pi/2$ flipper − Precession Field − $\pi/2$ flipper− −Sample− −$\pi/2$ flipper − Precession Field − $\pi/2$ flipper − Analyzer

In ferromagnetic NSE the beam is depolarized at the sample just like in "normal" NSE. If a precise knowledge of the polarization of the incident and scattered beams is required, additional polarizer and analyzer elements are placed around the sample, the so-called IMNSE sequence:

Polarizer (A) − $\pi/2$ flipper − Precession Field − $\pi/2$ flipper − Polarizer (B)− −Sample (π flipper)− −Analyzer (A) − $\pi/2$ flipper − Precession Field − $\pi/2$ flipper − Analyzer (B)

The components before and behind the sample are identical. The wavelength-dependent polarization at the end of each precession area is given by Eq. (3). The polarizer/analyzer devices behind each IMNSE branch transmit only one, e.g. $|+\rangle$, state leading to a wavelength-dependent transmission:

$$T(I,\lambda) = P_0\frac{(1+\cos(aI\lambda))}{2} \tag{4}$$

Fig. 1 shows the resulting intensity modulated beams as a function of the wavelength for $P_0 = 1$ and a Gaussian wavelength distribution:

$$g(\lambda) = \frac{1}{\sqrt{2\pi\sigma^2}}\exp\left(-\frac{(\lambda-\lambda_0)^2}{2\sigma^2}\right) \tag{5}$$

with $\lambda_0 = 4.5\,\text{Å}$ and $\Delta\lambda/\lambda = 2\sigma\sqrt{2\ln(2)} = 0.15$. If the sample does not change the polarization of the beam, the IMNSE signal $I_{\mathrm{IMNSE}}(\Delta I)$ can be calculated from the total transmission of the set-up if the balance in the magnetic field integrals before and behind the sample is modified by a symmetry adjustment or a phase coil, which is placed in the incoming beam in Fig. 3:

$$\frac{I_{\mathrm{IMNSE}}(\Delta I)}{I_0} = \int T_1(I+\Delta I,\lambda)T_2(I,\lambda)g(\lambda)\,\mathrm{d}\lambda \tag{6}$$

where I_0 is the intensity of the incoming beam behind the polarizer (A). The result is shown in Fig. 2. At the sample the intensity is $I_{\mathrm{sample}} = I_0/2 = I_+$ because only one state is transmitted by the polarizer (B). At the analyzer (B) and with respect to I_0 the echo ideally has an amplitude of 0.125 and a mean of 0.25, as expected from the product of the averaged transmissions $\langle T_1\rangle\langle T_2\rangle$.

INMSE is a powerful technique because it completely disconnects the sample area and the NSE measurement and can be

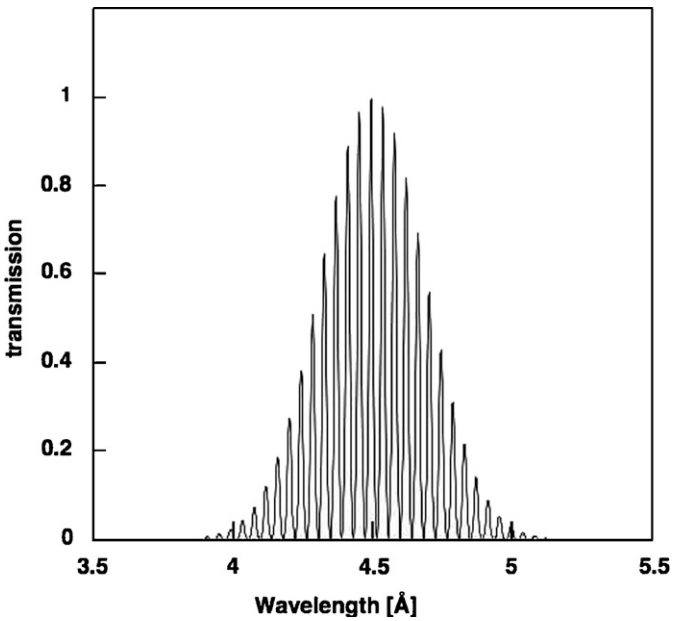

Fig. 1. Wavelength dependence of the transmission of the sequence "$\pi/2$ flipper–precession field-$\pi/2$ flipper–polarizer" given by Eq. (4) for ideal polarization conditions: 100% polarization for the incoming beam and 100% polarizer and flipper efficiency. The mean wavelength is 4.5 Å and the Gaussian wavelength distribution has a width of $\Delta\lambda/\lambda = 0.15$ FWHM.

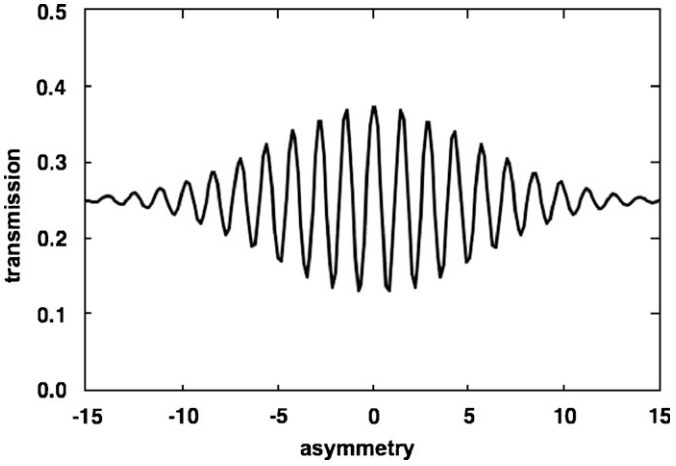

Fig. 2. Neutron spin echo group calculated from Eq. (6). It is the ideal transmission function of an IMNSE set-up assuming 100% polarization for the incoming beam and 100% efficiency of the polarizers and analyzers.

used for samples that completely depolarize the beam [12]. It can also access the spin-flip and non-spin-flip channels separately and thus allows for a separate analysis of, e.g. coherent and spin incoherent contributions. However, the unambiguous separation of nuclear and magnetic signals, which is inherent in NSE, is no longer possible with IMNSE.

The polarimetric NSE set-up is a variant of the IMNSE configuration, which uses the Cryopad to control the polarization around the sample and does not need the additional polarizer behind the sample:

Polarizer (A) – $\pi/2$ flipper – Precession Field – $\pi/2$ flipper – Polarizer (B)–
–Incident Nutator – Cryopad (Sample) – Outgoing Nutator–
$\pi/2$ flipper – Precession Field – $\pi/2$ flipper – Analyzer (B)

Fig. 3 shows a schematic set-up, with the sample placed in the zero-field chamber of Cryopad. The polarizer in front of the sample was a solid-state compact polarizer produced at HMI [16]. The incident polarization direction was defined by the compact polarizer and Cryopad (incident nutator plus incident precession coil). Similarly, the Cryopad selects the outgoing polarization direction and supersedes an additional polarizer behind the sample. If a π flip is needed, it will suffice to flip the direction of the incident or outgoing directions of polarization with the nutators of Cryopad.

As mentioned above, the polarimetric NSE gives a maximum echo amplitude of 1/8 with respect to I_O. This is only a factor of 2 less that in paramagnetic NSE, where the echo amplitude is 1/4 [4,18]. In reality this factor is closer to 3 due to additional intensity losses from the finite transmission of the polarizer (B).

The third generation Cryopad [9] is shown in Fig. 4. The Cryopad and the matching Orange cryostat that fits in it came from the Institut Laue-Langevin in Grenoble, France, and the experiment was carried out at the Wide Angle NSE Spectrometer SPAN [17] of BENSC, at the Hahn-Meitner Institut in Berlin, Germany. This joint ILL-HMI experiment was part funded under of the Polarized Neutron Techniques Joint Research Activity of the EU FP6-NMI3 Program.

3. Data acquisition and treatment

Measurements and data reduction are identical for polarimetric and conventional NSE [11,18]. The echo was measured by scanning the current in the phase coil (see Fig. 3) and by measuring four points separated by 90° in phase as shown in Fig. 5. The echo in Fig. 5 shows a minimum in contrast to the group calculated in Fig. 2. It is common practice to convert an echo maximum to a minimum by changing the polarity of one $\pi/2$ flipper and to measure around the minimum to improve statistics. The intensities of the four echo points are given by the formula (see Fig. 5):

$$I_i = I_{\text{average}} - I_{\text{echo}} \sin\left(\theta + (i-1)\frac{\pi}{2}\right) \tag{7}$$

with $i = 1,2,3$ and 4. The parameter I_{average} is obtained with high accuracy as the mean value of the four points. There are several ways to derive the echo amplitude I_{echo}. The most straightforward method is to calculate the mean square deviation of the four echo points. This easy echo calculation can never give a zero or negative echo and obviously overrates the echo amplitude, when the signal over noise ratio gets small. For this reason more sophisticated algorithms have been developed, which impose Eq. (7), and may fix the phases to values determined by reference measurements [19].

In the quasi-elastic approximation ($\omega \ll \omega_o$, with ω the energy transfer and ω_o the incident energy) the echo amplitude I_{echo} is the cosine Fourier transform of $S(\vec{Q},\omega)$, i.e. the real part of the time-dependent correlation function, the so-called intermediate scattering function $I(\vec{Q},\omega)$:

$$I_{\text{echo}} = \text{Re}I(Q,t) = \int S(Q,\omega)\cos(\omega t)\,\mathrm{d}\omega \tag{8}$$

Thus, the echo polarization is the intermediate scattering function normalized by the static structure factor, $S(Q,t=0) \equiv S(Q) \propto I_+ - I_-$, where I_+ and I_- are the intensities for the states $|+\rangle$ the $|-\rangle$, respectively, which are determined separately. We note at this point that the static structure factor determined in this way depends on the transmission band of the spectrometer (analyzers, polarizers, detector efficiency) and is therefore a kind of quasi-elastic structure factor $S_{\text{qe}}(Q)$ missing the high-energy excitations.

$$P_{\text{NSE}} \equiv \frac{I_{\text{echo}}}{I_+ - I_-} = \frac{\text{Re}I(Q,t)}{S_{\text{qe}}(Q)} \tag{9}$$

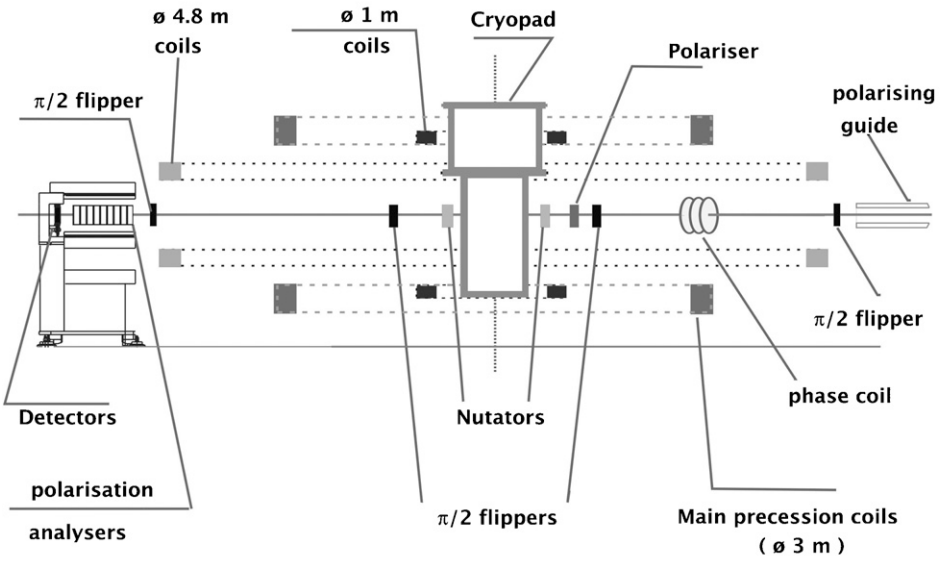

Fig. 3. Schematic drawing of the set-up seen from the side with the coils of SPAN and the elements required for the polarimetric set-up: additional polarizer, Cryopad and nutators. Note the presence of the phase coil at the incoming beam, which changes the symmetry in the magnetic field integrals between the two branches of the spectrometer so that the echo signal can be recorded.

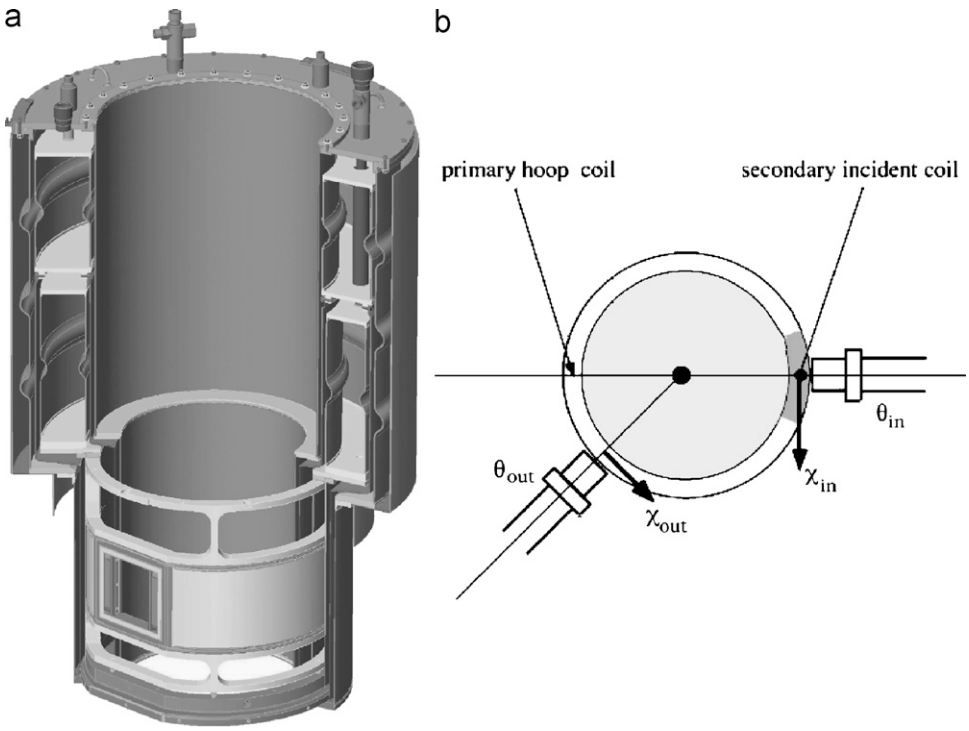

Fig. 4. The 3D representation of the Cryopad and schematic view from the top of the precession coils inside the Meissner shields.

By definition Eq. (9) obeys the relation $S(\vec{Q}, t = 0) = 1$ and is identical to the Kubo relaxation function. As in conventional NSE, the resolution is taken into account by calibration measurements of an elastic reference sample. The normalized intermediate scattering function is obtained from the measured signal through

$$S(Q,t) = \frac{P_{\text{sample}}}{P_{\text{reference}}} = \frac{[I_{\text{echo}}/(I_+ - I_-)]_{\text{sample}}}{[I_{\text{echo}}/(I_+ - I_-)]_{\text{reference}}} \tag{10}$$

i.e. the correction for instrumental effects is a simple division with no model function assumed.

4. Magnetic field configuration

The magnetic field of SPAN is created by three pairs of coils, with diameters of 1, 3 and 4.8 m, respectively, shown in Fig. 3 (from the side) and Fig. 6 (from the top). All pairs of coils are mounted in a Helmholtz fashion, one coil above and one coil below the scattering plane. In all pairs the electric currents are antiparallel. The configuration of SPAN has a cylindrical symmetry and the magnetic field integral is independent of the scattering angle, opening up a wide range of scattering angles for simultaneous NSE measurements. The cylindrical symmetry also

ensures a low-field area around the sample, which is an ideal configuration for the installation of Cryopad.

The main contribution to the precession field of SPAN comes from the ∅ 3 m coils, which produce a horizontal magnetic field in the scattering plane. The magnitude of the field depends on its distance from the center of symmetry, which is the sample position, where the magnetic field is zero. The coils with a diameter of 1 m normally lift the zero magnetic field point out of the scattering plane by producing a weak homogeneous vertical field of 0.2–0.3 mT at the sample, which assures the axial symmetry of the magnetic configuration [20]. In the polarimetric NSE set-up the 1 m coils ideally compensate the field of the main coils around the sample, so that the zero-field chamber defined by the Meissner and μ-metal shields of Cryopad can be accommodated. The coils with diameter of 4.8 m adjust the axial component of the field at the position of the outer $\pi/2$ flippers, which are also needed for conventional NSE measurements.

The spectrometer SPAN was relocated in the new Neutron Guide Hall of BENSC-HMI [21] and recommissioned in early 2007. The mechanical mounting and alignment of the precession coils were improved and resulted in a more homogeneous magnetic field. A genetic algorithm coupled to a model of the magnetic field configuration of the spectrometer calculated using the software package RADIA [22] was employed to find the ideal positions and currents of the coils, which were very close to the original design. For the first time artificial intelligence algorithms were used to optimize a neutron spectrometer and this pioneering approach opens up new opportunities for the application of evolutionary algorithms to the design of scientific instruments [23].

For each current value in the main coils of SPAN, the genetic algorithm optimized the currents in the other coils in order to minimize the field at field-sensitive points in the spectrometer and Cryopad. A model of the instrument showed that at a current of 60 A in the main coils of SPAN (∼1/6th of the nominal resolution) the edges of the μ-metal shielding begin to saturate, which was the limiting criterion used in the algorithm. These RADIA calculations were crosschecked and confirmed by finite-element calculations made at ILL using the ANSYS software.

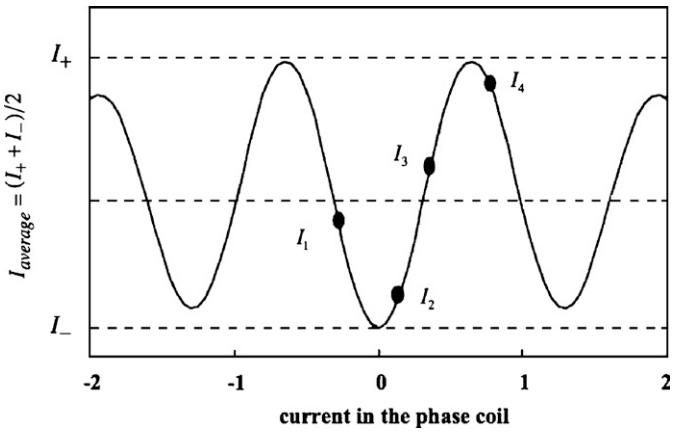

Fig. 5. Neutron spin echo signal as a function of the current in the phase coil, which changes the balance in the magnetic field integrals between the two branches of the spectrometer. The amplitude and position of the echo are determined by measuring at least four points, with a step of 90° in phase, around the optimum.

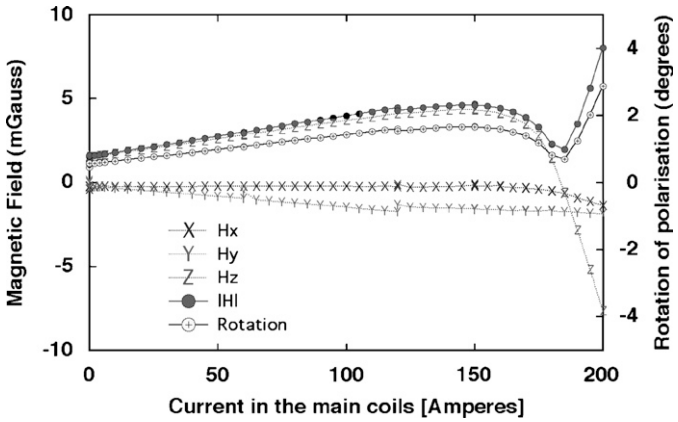

Fig. 7. All three components of the magnetic field (Hx, Hy, Hz) inside the zero-field chamber of Cryopad measured with a Bartington flux gate probe. The measured values and the calculated modulus of the field $|\vec{H}|$ are plotted as a function of the current in the primary coil of the spectrometer SPAN. For each current value, the currents injected in the ∅ 1 and ∅ 4.8 m coils were set in a way that the field map remains optimum. The expected rotation of polarization in the zero-field chamber remains lower than 2° at 4.5 Å up to 180 A. The right-handed cartesian set is chosen with $\vec{x}$ parallel to $\vec{Q}$, $\vec{y}$ in the horizontal scattering plane and $\vec{z}$ vertical.

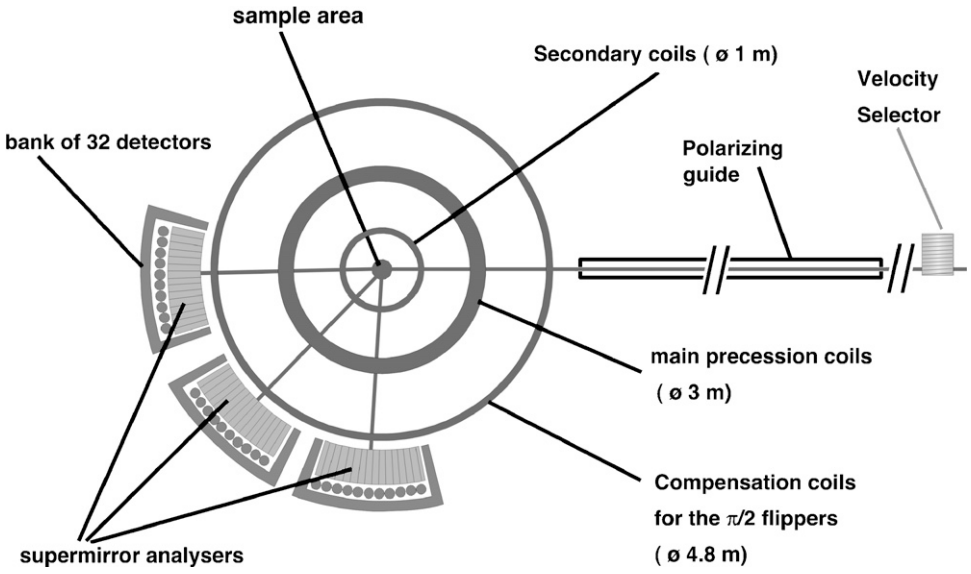

Fig. 6. View of the wide angle NSE spectrometer SPAN from the top with the precession coils (∅ 1, ∅ 3 and ∅ 4.8 m) and the detector banks.

These criteria turned out to be pessimistic. When the Cryopad was installed at SPAN for the first time, all three components of the magnetic field were monitored inside the zero-field chamber by a Bartington Flux Gate Probe. As shown in Fig. 7, the magnetic field inside the Cryopad only started to increase considerably (50% of the nominal resolution), after the current inside the coils had reached 180 A

5. Set-up and reference measurements

The measurements were done at a wavelength of 4.5 Å with a monochromatization of $\Delta\lambda/\lambda$ ~0.15 delivered by the velocity selector of SPAN. On SPAN the beam has a vertical divergence of $\pm 1.2^\circ$ and each detector has an opening of 0.8°. The total angular opening for simultaneous measurements was 3.2° (i.e. 4 detectors) and was limited by the opening of the nutators of the cryopad after the sample. The set-up was optimized on a Grafoil sample, which is a strong coherent elastic SANS scatterer commonly used in NSE [24]. We started with the standard NSE configuration of SPAN and the successive steps described below and summarized in Fig. 8 led to the arrangement schematically shown in Fig. 9. After each step the settings were checked for each value of the current inside the main coils.

5.1. Ferromagnetic NSE

The two additional $\pi/2$ flippers were placed at a distance of ~60 cm from the sample, the minimum distance to the sample which left enough space for the additional polarizer/analyzer and the Cryopad. At this position, however, the $\pi/2$ flippers were located outside the ∅ 1 m coils (see Fig. 3) in a high magnetic field area. Thus, additional compensation coils were required. The upper limit for the magnetic field integral of this configuration was defined by the fact that the efficiency and homogeneity of this compensation fails at a current of ~100 A in the ∅ 3 m coils of SPAN.

5.2. IMNSE

After successful completion of the ferromagnetic NSE installation, the solid-state compact polarizer with an overall length of

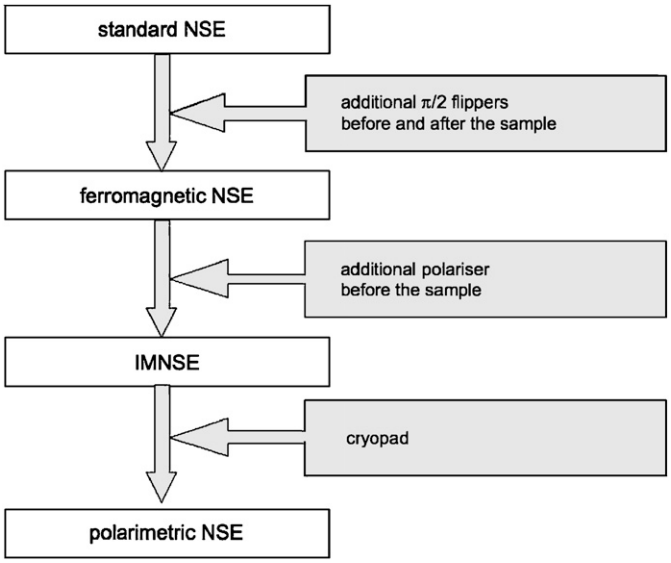

Fig. 8. Representation of the successive steps and components needed to transform an NSE configuration to Polarimetric NSE.

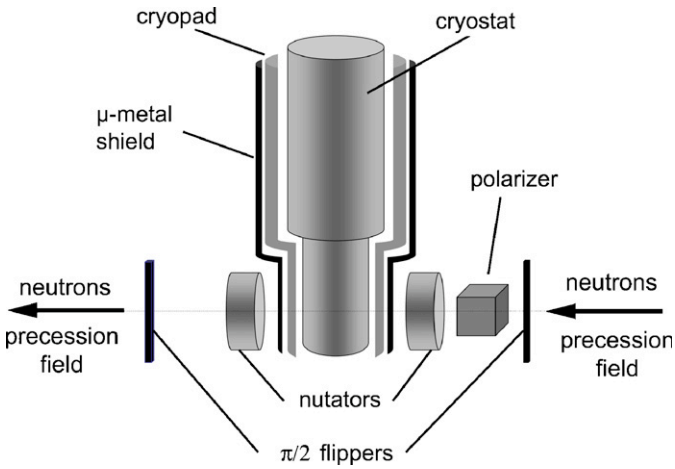

Fig. 9. Schematic view of the arrangement around the sample position with additional $\pi/2$-flippers, polarizer, nutators and Cryopad.

9 cm was placed in the incoming beam about ~5 cm behind the second $\pi/2$-flipper. Permanent magnets produced a strong vertical magnetic field of almost 0.1 T inside the polarizer, which was required for the complete saturation of the FeSi/Si supermirrors. Unfortunately, the resulting stray field on the neighboring $\pi/2$ flipper was too much strong and therefore the field was shielded with Fe plates placed around the polarizer. However, this also reduced the amplitude of the field inside the polarizer. The best compromise led to ~0.015 T in the polarizer, a polarization of 95%, and the same resolution as for the ferromagnetic NSE set-up.

5.3. Polarimetric NSE

In a last step Cryopad and its nutators were installed and the adiabatic transport of the polarization at different positions of the nutators were checked. With the Grafoil in the zero-field chamber of Cryopad, only the diagonal terms (P_{xx}, P_{yy}, P_{zz}) could be measured, because this sample exhibits only nuclear scattering and does not rotate the initial polarization of the beam. Fig. 10 shows the echo P_{NSE} as obtained from Eq. (11) versus the Fourier time (t) for the three diagonal terms. These spectra correspond to a reference or resolution function of the set-up and coincide with each other, confirming the complete decoupling of Cryopad from the precession fields of SPAN. The echo amplitude decreases at high fields and Fourier times, as well at the shortest Fourier times. At very low magnetic fields, the echo is reduced due to the stray field of the polarizer before the sample, next to the $\pi/2$ flipper.

6. The case of MnSi

The first polarimetric NSE measurements on a complex magnetic system were done with a well-characterized MnSi single-crystal sample [25]. MnSi is an itinerant magnet which orders below ~29 K into a left-handed helical structure with a period of ~175 Å and a wavevector of 0.039 $Å^{-1}$ along the $\langle 1\,1\,1\rangle$ directions [26]. The helical structure is stabilized by the combination of a weak anisotropic exchange interaction and the asymmetric Dzyaloshinski–Moriya interaction due to the lack of inversion symmetry in the $P2_13(T_4)$ structure. The long period of the helix leads to purely magnetic Bragg peaks in the small angle area around the (0 0 0) point at $|\vec{Q}| = 0.039\,Å^{-1}$. Polarized neutrons have played a key role in the understanding of the magnetic structure and the determination of the handiness of the magnetic helix [25,27].

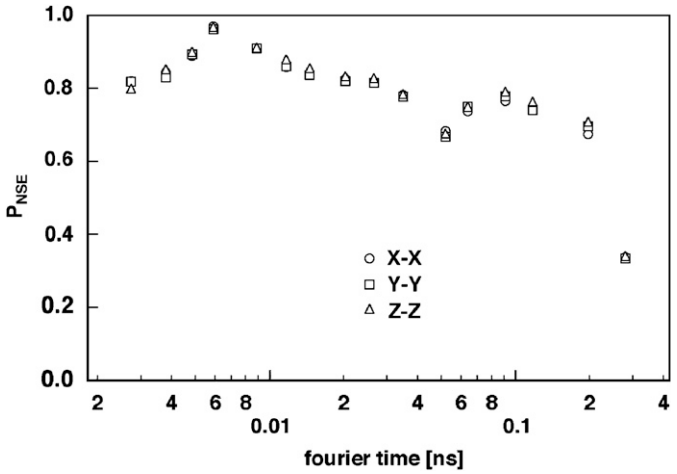

Fig. 10. Resolution curve recorded with a Grafoil sample, a strong coherent elastic SANS scatterer commonly used in NSE. Only the diagonal terms (P_{xx}, P_{yy}, P_{zz}) are non-zero, as expected from coherent elastic scattering and can be measured because the polarization is zero for all cross terms. The right-handed cartesian set is chosen with $\vec{x}$ parallel to $\vec{Q}$, $\vec{y}$ in the horizontal scattering plane and $\vec{z}$ vertical.

Due to the discovery of a quantum phase transition under applied pressure, the magnetic properties of MnSi have recently attracted much attention [28]. At ambient pressure, MnSi has a very simple helix structure with the spins perpendicular to the propagation vector of the helix $\vec{\tau}$ along one of the $\langle 111 \rangle$ crystallographic directions. This is exactly the simple helical structure considered by Blume in his historical paper [1] to illustrate the non-trivial repercussions of his theory on the scattering of polarized neutrons. The Mn atoms are located on the 4a site with $x = 0.138$. The helix can be described by two orthogonal vectors $\vec{S}_1$ and $\vec{S}_2$, which have the same amplitude and lie in a plane perpendicular to $\vec{\tau}$. The magnetic structure factor for a reflection $\vec{K}$ is given by (see [9]) $M(\vec{K}) = \sum_j \vec{m}_j f(\vec{K}) \exp(2\pi \vec{K} \vec{r}_j)$, where $\vec{m}_j = (1/2)\mu(\vec{S}_1 - i\vec{S}_2) \exp(2i\pi\vec{\tau}g\vec{r}_j) \exp(i\phi_j)$, μ is the amplitude of the Mn moments, f the magnetic form factor of the Mn atoms, $\vec{r}_j$ an atomic position and ϕ_j an arbitrary phase angle. Because the magnetic interaction vector $\vec{M}_\perp(\vec{K}) = \vec{K} \wedge \vec{M}(\vec{K}) \wedge \vec{K}$ is the projection of the magnetic structure factor onto a plane perpendicular to the scattering vector $\vec{K} = \vec{Q}$, it is convenient to choose the set of orthogonal polarization axes with $\vec{x}$ parallel to $\vec{Q}$, $\vec{z}$ conventionally perpendicular to the scattering plane and $\vec{y}$ completing the right-handed Cartesian set. During the experiment, we measured one of the four equivalent magnetic reflection 000+τ, where $\tau = (0.039, 0.039, 0.039)$. The magnetic Bragg peak intensity was covering one detector with an opening of 0.8° and $\Delta Q = 0.0195\,\text{Å}^{-1}$. The MnSi sample was oriented so that $\vec{x} \| (1,1,1)$ (i.e. $\vec{Q}$) and $\vec{z} \| (1,\bar{1},1)$. For this reflection, the intensity of the diffracted beam is proportional to

$$\sigma = \vec{M}_\perp \vec{M}_\perp^* + \vec{P}_i \Im\left(\vec{M}_\perp \wedge \vec{M}_\perp^*\right) \tag{11}$$

and the scattered polarization is defined as

$$\vec{P}_f \sigma = -\vec{P}_i(\vec{M}_\perp \vec{M}_\perp^*) + 2\Re((\vec{P}_i \cdot \vec{M}_\perp^*)\vec{M}_\perp) - \Im(\vec{M}_\perp \wedge \vec{M}_\perp^*) \tag{12}$$

The above two equations easily show that the scattered polarization $\vec{P}_f \| -\vec{x}$, if $\vec{P}_i$ is successively parallel to $\vec{x}, \vec{y}$ or $\vec{z}$ and that there is no reflection, if $\vec{P}_f \| \vec{x}$. In other words, the effect of the helix appears provided that the incident polarization is antiparallel to $\vec{Q}$ and that it is in the helix plane, i.e. perpendicular to $\vec{\tau}$ (or $\vec{Q}$). In the latter case the polarization rotates by 90°.

The polarization matrix elements were analyzed in the low-temperature helical and the paramagnetic phases. Figs. 11 and 12 show the echo groups measured at the Bragg peak of the helix for the spin-flip configuration ($\vec{P}_i \| \vec{x}, \vec{P}_f \| -\vec{x}$) and for the cross term ($\vec{P}_i \| \vec{z}, \vec{P}_f \| -\vec{x}$, i.e. 90° rotation), respectively. The solid lines are fits with the wavelength and a fixed 15% monochromatization of the beam. It is remarkable and an interesting side effect of the poor Q resolution inherent in very low-angle scattering that the magnetic Bragg peak does not affect the very broad monochromatization (15%) of the incident beam.

Fig. 13 shows the polarimetric NSE resolution measured at the magnetic Bragg peak at 6 K for the configuration ($\vec{P}_i \| /\vec{x}, \vec{P}_f \| -\vec{x}$) and for the cross terms. The data are nicely congruent and thus confirm the decoupling of the sample area as seen on the Grafoil spectra from the NSE measurement. It is worth noting that the decay of the resolution at short and long times is less pronounced in Fig. 13 than in Fig. 10, showing that the slight improvements of the set-up, which were performed between these two measurements, greatly benefited the shape of the resolution.

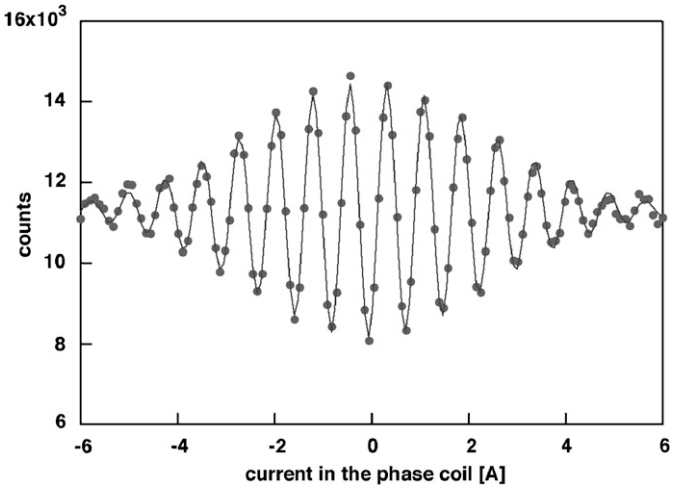

Fig. 11. Polarimetric neutron spin echo group recorded on the helimagnetic Bragg peak of MnSi at 25 K in the spin-flip configuration with the incoming polarization along the scattering vector $\vec{Q}$ and the outgoing polarization along $-\vec{Q}$.

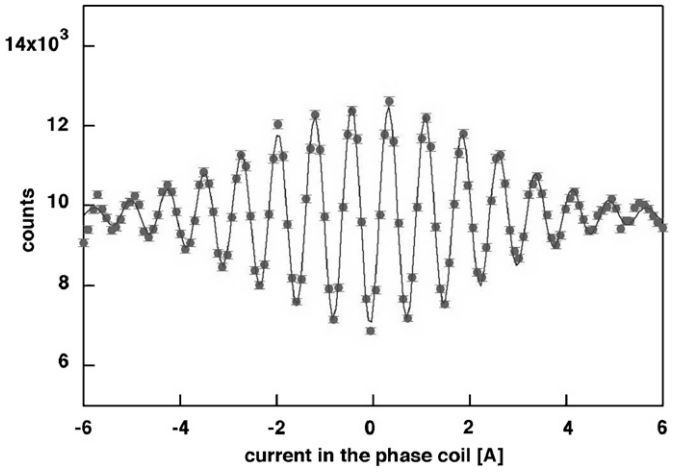

Fig. 12. Polarimetric neutron spin echo group recorded on the helimagnetic Bragg peak of MnSi at 25 K for a 90° rotation of the polarization with the incoming polarization along the beam propagation vector and the outgoing polarization along $-\vec{Q}$.

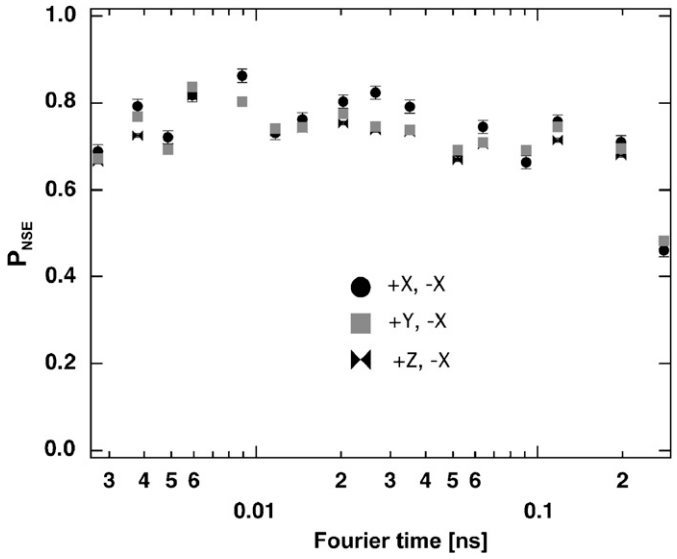

Fig. 13. Polarimetric NSE polarization recorded on the Bragg peak at $Q = 0.036\,\text{Å}^{-1}$ of the helical magnet MnSi at 6 K. The elastic signal is measured for the spin-flip configuration $\vec{P}_{i\parallel}\vec{Q}\cdot\vec{P}_{f\parallel}-\vec{Q}$ configuration and for the crossed terms $\vec{P}_{i}\perp\vec{Q}\cdot\vec{P}_{f\parallel}-\vec{Q}$. The right-handed cartesian set is chosen with $\vec{x}$ parallel to $\vec{Q}$, $\vec{y}$ in the horizontal scattering plane and $\vec{z}$ vertical.

The NSE spectra of MnSi were analyzed as a function of temperature up to and exceeding T_C. However, in the paramagnetic phase the intensity of the helical peak decreases rapidly and careful background corrections are required. These results will be reported later.

7. Conclusions

These initial results show that it is possible to completely decouple the precession field areas of an NSE spectrometer from the zero-field chamber of Cryopad. State-of-the-art SNP can therefore be combined with NSE spectroscopy without any reservations at the expense of some intensity loss due to the additional polarizer device. The compact and most efficient design greatly benefits from recent developments in the field of compact optical elements for polarized neutrons. The success of these first measurements demonstrates the feasibility of the method and opens up new opportunities for polarized neutron spectroscopy. We are confident that Polarimetric NSE will be developed further and become the method of choice for a deeper understanding of chiral and other complex magnetic phase transitions.

Acknowledgments

The Cryopad arrived damaged in Berlin. The authors thank the HMI sample environment team in particular Christof Fritsche for the fast and efficient repair. The authors also acknowledge the technical support by R. Kischnik, C. Rethfeld, P. Granz, N. Beul, H.-P. Schneider, P. Mertens, K.H. Degenhardt and L. Rossa. Special thanks to Thomas Krist for lending his compact solid-state polarizer and to Francis Tasset, inventor of Cryopad, with whom we have had very fruitful discussions. Last but not the least, the authors thank the Neutrons and Muons Integrated Infrastructure Initiative (NMI3) of the EU 6th Framework Programme (FP6) for the financial support through the Key Action "Strengthening the European Research Area, Research Infrastructures" Contract no: HII3-CT-2003-505925.

References

[1] M. Blume, Phys. Rev. 130 (1963) 1670.
[2] S.V. Maleyev, V.G. Bar'jakhtar, R.A. Suris, Sov. Phys. Solid State 4 (1963) 2533.
[3] R.M. Moon, T. Riste, W.C. Koehler, Phys. Rev. 181 (1969) 920.
[4] A.P. Murani, F. Mezei, in: F. Mezei (Ed.), Neutron Spin Echo, Lecture Notes in Physics Series, vol. 128, Springer, Heidelberg, 1980, p. 104.
[5] H. Alperin, in: International Conference on Magnetism, Proc. ICM-731973, Moscow, 1973.
[6] M.Th. Rekveldt, J. Phys. Collq. C1 (1971) 579.
[7] G. Drabkin, A. Okorokov, V. Runov, JETP Lett. 15 (1972) 324;
A. Okorokov, V. Runov, A. Gukasov, Nucl. Instr. and Meth. 157 (1978) 487.
[8] F. Tasset, Physica B 156–159 (1989) 627.
[9] E. Lelièvre-Berna, et al., Physica B 356 (2005) 131;
E. Lelièvre-Berna, Physica B 397 (2007) 120.
[10] M. Janochek, S. Klimko, R. Gähler, B. Roessli, P. Böni, Physica B 397 (2007) 125.
[11] F. Mezei, C. Pappas, Th. Gutberlet (Eds.), Neutron Spin Echo Spectroscopy, Lecture Notes in Physics Series, vol. 601, Springer, Heidelberg, 2003.
[12] B. Farago, F. Mezei, Physica B 136 (1986) 627.
[13] F. Mezei, Physica B 151 (1988) 74.
[14] R. Gähler, R. Golub, K. Habicht, T. Keller, J. Felber, Physica B 229 (1996) 1.
[15] F. Mezei, A. Ioffe, G. Drabkin, Physica B 297 (2001) 9.
[16] T. Krist, Nucl. Instr. and Meth. Phys. Res. A 529 (2004) 50.
[17] C. Pappas, G. Kali, T. Krist, P. Böni, F. Mezei, Physica B 283 (2000) 365.
[18] C. Pappas, F. Mezei, G. Ehlers, in: T. Chatterji (Ed.), Neutron Scattering from Magnetic Materials, Elsevier, Amsterdam, 2006, p. 521.
[19] G. Ehlers, B. Farago, Private communication.
[20] C. Pappas, F. Mezei, J. Neutron Res. 5 (1996) 35.
[21] D. Clemens, C. Pappas, Th. Krist, H-J. Bleif, J. Peters, F. Mezei, Layout and performance of the new neutron guide bundle at BENSC, in: European Workshop on Neutron Optics (NOP'07), Villigen (Schweiz), 5.–7.3.07.
[22] 〈http://www.esrf.eu/Accelerators/Groups/InsertionDevices/Software/Radia〉;
O. Chubar, P. Elleaume, J. Chavanne, J. Synchrotron Rad. 5 (1998) 481–484.
[23] P.M. Bentley, C. Pappas, K. Habicht, E. Lelievre-Berna, Physica B 385–386 (2006) 1349–1351.
[24] These samples have been provided to the NSE community by M. Monkenbusch.
[25] S.V. Grigoriev, et al., Phys. Rev. B 72 (2005) 134420;
S.V. Grigoriev, et al., Phys. Rev B 74 (2006) 214414.
[26] Y. Ishikawa, K. Tajima, D. Bloch, M. Roth, Solid State Commun. 19 (1976) 525
P.A. Hansen, Risø Report Nr. 360 (Thesis), Risø National Laboratory, Gjellerup, Copenhagen, 1977.
[27] M. Ishida, et al., J. Phys. Soc. Japan 54 (1985) 2975.
[28] U.J. Uemura, et al., Nat. Phys. 3 (2007) 29.